



Article

Facile Construction of All-Solid-State Z-Scheme $g\text{-C}_3\text{N}_4/\text{TiO}_2$ Thin Film for the Efficient Visible-Light Degradation of Organic Pollutant

Wan Zhao ¹, Xiuru Yang ¹, Chunxi Liu ¹, Xiaoxiao Qian ¹, Yanru Wen ¹, Qian Yang ¹, Tao Sun ¹, Wenyang Chang ¹, Xin Liu ^{2,*} and Zhi Chen ^{1,*}

¹ College of Materials and Chemistry, China Jiliang University, 258 Xueyuan Street, Xiasha Higher Education District, Hangzhou 310018, China; 17826827277@163.com (W.Z.); yxr15957119921@126.com (X.Y.); 15867130507@163.com (C.L.); qxiao1116@126.com (X.Q.); czmichael@hotmail.com (Y.W.); czmichael@163.com (Q.Y.); 15958003262@163.com (T.S.); 18757556442@163.com (W.C.)

² College of Standardization, China Jiliang University, 258 Xueyuan Street, Xiasha Higher Education District, Hangzhou 310018, China

* Correspondence: liuxin@cjlu.edu.cn (X.L.); zchen0@gmail.com (Z.C.); Tel.: +86-571-87676395 (X.L.); +86-571-86835738 (Z.C.)

Received: 19 February 2020; Accepted: 21 March 2020; Published: 25 March 2020



Abstract: The increasing discharge of dyes and antibiotic pollutants in water has brought serious environmental problems. However, it is difficult to remove such pollutants effectively by traditional sewage treatment technologies. Semiconductor photocatalysis is a new environment-friendly technique and is widely used in aqueous pollution control. TiO_2 is one of the most investigated photocatalysts; however, it still faces the main drawbacks of a poor visible-light response and a low charge-separation efficiency. Moreover, powder photocatalyst is difficult to be recovered, which is another obstacle limiting the practical application. In this article, $g\text{-C}_3\text{N}_4/\text{TiO}_2$ heterojunction is simply immobilized on a glass substrate to form an all-solid-state Z-scheme heterojunction. The obtained thin-film photocatalyst was characterized and applied in the visible-light photodegradation of colored rhodamine B and tetracycline hydrochloride. The photocatalytic performance is related to the deposited layers, and the sample with five layers shows the best photocatalytic efficiency. The thin-film photocatalyst is easy to be recovered with stability. The active component responsible for the photodegradation is identified and a Z-scheme mechanism is proposed.

Keywords: thin-film photocatalyst; environmental control; antibiotic residue removal; $g\text{-C}_3\text{N}_4/\text{TiO}_2$; all-solid-state Z-scheme heterojunction

1. Introduction

Water pollution has become particularly serious in recent decades due to the rapid development of industrialization [1]. The photocatalytic technique provides an alternative strategy to solve the above problem since it converts solar energy directly into useful energy for degrading organic pollutants into harmless components [2]. In 1977, Frank reported [3] the successful degradation of pollutants in water by using TiO_2 as the photocatalyst, which aroused extensive applications of TiO_2 in water treatment. In 1987, Matthews et al. [4] found that 34 kinds of organic pollutants in water could be degraded by TiO_2 under the irradiation of ultraviolet light (UV-light). Until now, TiO_2 is one of the most popular photocatalysts for environmental protection [5,6].

However, pristine TiO_2 photocatalyst has two intrinsic defects of a wide bandgap (3.2 eV) and the fast recombination of photogenerated carriers, which limits its widespread development. It is necessary to modify pristine TiO_2 to simultaneously satisfy the requirements for practical applications

of photocatalytic techniques, such as intensive visible-light response, high photogenerated-carriers separation efficiency, good stability, and strong redox capabilities [7–9]. $g\text{-C}_3\text{N}_4$ is a recently emerged nonmetallic photocatalyst with a narrow bandgap (2.7 eV), demonstrating prominent features such as a visible-light response, good chemical stability, and easy synthesis [10–12]. Wang et al. [13] reported the efficient water splitting by using $g\text{-C}_3\text{N}_4$ as the visible-light photocatalyst in 2009. This has evoked great interests, and diverse approaches have been proposed to improve the photocatalytic efficiency. Among these strategies, construction heterojunction has been proven as one of the effective strategies [14]. In particular, TiO_2 and $g\text{-C}_3\text{N}_4$ can form an all-solid-state Z-scheme heterojunction due to their matched conduction band (CB) and valence band (VB) positions, which can not only overcome the intrinsic defects of pristine photocatalyst but can also maintain the strong redox ability [12,15]. Additionally, the powder photocatalyst is difficult to be recovered from the solution for further use, which is another obstacle restraining the wide application of the photocatalytic technique in water treatment [16–18]. Intensive efforts have been made to immobilize the powder photocatalyst on substrates such as aerogels or glass [19,20].

Herein, all-solid-state Z-scheme $g\text{-C}_3\text{N}_4/\text{TiO}_2$ thin-film photocatalysts were successfully constructed by using the common glass as the substrate from the simple sol-gel and spin coating process. The obtained thin-film photocatalysts show good photodegradation performances for the treatment of colored Rh B and colorless tetracycline hydrochloride under visible light, which are closely related to the coating layers. The active reagent is identified and a Z-scheme mechanism is proposed.

2. Experiment

2.1. Materials

All the chemicals were purchased from commercial suppliers and were used directly. Absolute ethanol (CH_5OH), isopropanol ($\text{C}_3\text{H}_8\text{O}$), glacial acetic acid (CH_3COOH), butyl titanate ($\text{C}_{16}\text{H}_{36}\text{O}_4\text{Ti}$), and tetracycline hydrochloride ($\text{C}_{22}\text{H}_{24}\text{N}_2\text{O}_8\cdot\text{HCl}$, TC-HCl) were obtained from Shanghai Aladdin Biochemical Technology Co. Ltd. (Shanghai, China). Melamine ($\text{C}_3\text{N}_3(\text{NH}_2)_3$) and tert butyl alcohol ($(\text{CH}_3)_3\text{COH}$, TBA) were bought from Wuxi Prospect Chemical Reagent Co. Ltd. (Wuxi, China). Benzoquinone ($\text{C}_6\text{H}_4\text{O}_2$, BQ) and ethylene diamine tetraacetic acid ($\text{C}_{10}\text{H}_{16}\text{N}_2\text{O}_8$, EDTA) were obtained from Shanghai Macklin Biochemical Technology Co. Ltd. (Shanghai, China). Rhodamine B ($\text{C}_{28}\text{H}_{31}\text{ClN}_2\text{O}_3$, RB) was purchased from Tianjin Kemio Chemical Reagent Co. Ltd. (Tianjin, China).

2.2. Preparation

Preparation of $g\text{-C}_3\text{N}_4$ powder. The preparation of $g\text{-C}_3\text{N}_4$ was operated according to the previous report [12]. Typically, 10.0 g of melamine was put into an alumina crucible and heated at 523 °C with a ramp rate of 2 °C/min in a muffle furnace under air atmosphere. Then, the solid was cooled down to room temperature after keeping at 523 °C for 4 h and ground to get $g\text{-C}_3\text{N}_4$ powder product.

Preparation of TiO_2 sol. The preparation TiO_2 sol was similar to the former publication [21]. Generally, it can be specifically divided into the following three steps: (1) 60 mL of absolute ethanol and 20 mL of butyl titanate were successively added into a 250 mL beaker at room temperature, and the mixture was stirred for 30 min to obtain a pale yellow transparent solution (recorded as beaker A); (2) 80 mL absolute ethanol, 20 mL deionized water, and 32 mL glacial acetic acid were successively put into 250 mL beakers at room temperature and stirred continuously with the magnetic force for 30 min, which was defined as beaker B. (3) The solution in beaker B was dropped into beaker A at the rate of 2 drops per second, and the solution was kept constantly stirring for 2h to obtain the sol. The molar ratios of the reagent for the synthesis of TiO_2 sol were set as follows: absolute ethanol: butyl titanate: deionized water: glacial acetic acid = 40:1:20:8.83. The prepared sol was aged at room temperature for three days and underwent the alcoholysis–hydrolysis–polycondensation reaction to form a stable gel.

Preparation of g-C₃N₄/TiO₂ thin film. Typically, (1) the cleaning of the glass substrate would be carried out as follows: the diced glass substrate (20 × 15 × 1 mm³) was washed under ultrasonic in isopropanol, deionized water, and anhydrous ethanol for 15 min in sequence. Then, the cleaned glass substrate was dried at 80 °C and put into a sealed container for future use. (2) In total, 24.0, 48.0, 145.0, 241.0 and 334.7 mg of g-C₃N₄ powder was added into 20 mL of TiO₂ sol that had aged for 3 days, respectively. Then, they were constantly kept magnetically stirring for 20 min to obtain g-C₃N₄/TiO₂ powder-sol with its mass ratio of 0.05, 0.1, 0.3, 0.5 and 0.7. (3) The cleaned glass substrate was stuck to the homogenizer, 200 μL g-C₃N₄/TiO₂ pre-formed sol was dipped on the substrate. The sol was spin-coated on the substrate by a low speed of 500 rpm/min for 10 s and a successive high speed of 4000 rpm/min for 30 s. The coated sample was dried at 80 °C on a heating platform for 5 min, then one layer of film was obtained and the sample was denoted as a 1-layer g-C₃N₄/TiO₂ thin film. Then, 3, 5, and 7 layers of g-C₃N₄/TiO₂ thin film with the mass ratio of 0.5 and 5 layers of pristine TiO₂ thin film were prepared by a similar spin-coating process and the obtained samples were denoted as 3-layer g-C₃N₄(0.5)/TiO₂, 5-layer g-C₃N₄(0.5)/TiO₂, 7-layer g-C₃N₄(0.5)/TiO₂, 5-layer TiO₂, respectively. In addition, 5 layers of spin-coated g-C₃N₄/TiO₂ thin films with different g-C₃N₄/TiO₂ mass ratios of 0.05, 0.1, 0.3, 0.7 were prepared in the same way, and the obtained products were named as 5-layer g-C₃N₄(0.05)/TiO₂, 5-layer g-C₃N₄(0.1)/TiO₂, 5-layer g-C₃N₄(0.3)/TiO₂, and 5-layer g-C₃N₄(0.7)/TiO₂, respectively. In addition, g-C₃N₄(0.5)/TiO₂ powder photocatalysts were also prepared from the similar preparation processes of g-C₃N₄/TiO₂ thin-film photocatalyst. All the prepared samples were heated at 450 °C for 2 h with a ramp rate of 2.5 °C/min and automatically cooled down to room temperature.

2.3. Characterization

X-ray diffraction (XRD) patterns were acquired from Bruker D2 PHASER X-ray diffractometer (Bruker, Karlsruhe, Germany) with Cu K α radiation in the range of 10–80°. Fourier transform infrared (FT-IR) spectra were analyzed on Bruker TENSOR 27 Fourier transform infrared spectrometer (Bruker, Karlsruhe, Germany). Scanning electron microscope (SEM) images were recorded on the Hitachi SU 8010 instrument (Hitachi, Tokyo, Japan). The Ultraviolet-visible diffuse reflectance spectrum (UV-vis DRS) was measured on Shimadzu UV-3600 UV-visible using BaSO₄ as the reference (Shimadzu, Kyoto, Japan).

2.4. Photocatalytic Activity Measurement

The photocatalytic activities of prepared g-C₃N₄/TiO₂ thin films were evaluated by the degradation of colored dye (rhodamine B, Rh B) and colorless antibiotic (tetracycline hydrochloride, TC-HCl) in water. A 300-W Xe lamp with a 420-nm filter was used as the visible light source (≥ 420 nm). The prepared thin-film photocatalysts were immersed into 50 mL of 5 mg·L⁻¹ Rh B solution and 50 mL of 5 mg·L⁻¹ TC-HCl, and the distance between the light source and the glass substrate was set as 13 cm. The photocatalytic analyses were operated at a constant temperature by a circulating cooling system. Before the light irradiation, the solution with the photocatalyst was magnetically stirred in darkness for 0.5 h to establish adsorption equilibrium. During the light irradiation, 3 mL of the reaction liquid was taken out every 30 min and the solution was analyzed by the UV1600 spectrophotometer to determine the residual concentrate. Then, the measured solution was poured back into the reaction solution to continue the photodegradation.

Antibiotic TC-HCl was employed for stability measurement. Thin-film photocatalyst was immersed into 50 mL TC-HCl (5 mg·L⁻¹) and the photodegradation was carried out in the same way as that of Rh B. After a light irradiation of 180 min, the thin-film photocatalyst was taken out and washed with de-ionized water. Then, it was immersed into TC-HCl solution for another cycle of photodegradation, and 5 cycles were run in a similar fashion. As a comparison, a blank experiment without the photocatalyst was done in a similar fashion to study the photo-resistance of Rh B and TC-HCl.

2.5. Trapping Experiment

The active species responsible for the photodegradation were identified by the trapping experiments. Diverse trapping agents such as TBA, BQ, EDTA were separately added into the reaction solution (Rh B, $5 \text{ mg}\cdot\text{L}^{-1}$) and the same operation as the above photodegradation was done.

3. Results and Discussions

3.1. Structure, Composition, and Morphology

Figure 1A shows XRD patterns of the synthesized $\text{g-C}_3\text{N}_4$ and two distinct diffraction peaks at 12.9° and 27.6° , corresponding to the (100) and (002) crystal planes of $\text{g-C}_3\text{N}_4$ (PDF#87-1526) [22]. The same diffraction bands were also observed on other $\text{g-C}_3\text{N}_4$ -containing samples. As for the TiO_2 -containing photocatalysts (Figure 2B), the characteristic signals of anatase phase TiO_2 (PDF#21-1272) are presented, and no characteristic peaks associated with the rutile phase are observed in any of the samples. Compared with the 5-layer $\text{g-C}_3\text{N}_4(0.5)/\text{TiO}_2$, the peak of powder $\text{g-C}_3\text{N}_4(0.5)/\text{TiO}_2$ has much sharper (101), (004), (200), (105), (211), crystal planes that all corresponds to clear peaks, which indicates the latter has higher crystallinity [23]. However, it is difficult to observe the clear diffraction bands from $\text{g-C}_3\text{N}_4$, which should be resulted from its low quantity and high dispersion in the thin film.

The FT-IR spectra of the prepared photocatalysts are shown in Figure 2. Characteristic peaks at 1640 , 1409 , 1321 , and 1242 cm^{-1} can be clearly identified on $\text{g-C}_3\text{N}_4$, which are assigned to the stretching vibration of the aromatic CN heterocycle [24]. Additional peaks at 809 and $3100\text{--}3500 \text{ cm}^{-1}$ can be attributed to the typical triazine ring vibration and the stretching vibration of $\text{N}_2\text{H-}$ and -OH [25]. As for 5-layer TiO_2 , the peaks at about 3400 and 1630 cm^{-1} are assigned to the bending and stretching vibration of OH from the adsorbed water, respectively, which is similar with the previous report [26]. Additionally, the characteristic absorption peak of the TiO_2 thin film detected in the wavelength range of $450\text{--}700 \text{ nm}$ may be attributed to the stretching vibration of the Ti–O–Ti bond [27]. Only weak characteristic peaks of the $\text{g-C}_3\text{N}_4$ in 5-layer $\text{g-C}_3\text{N}_4(0.5)/\text{TiO}_2$ are detected in the FT-IR spectrum due to its low quantity.

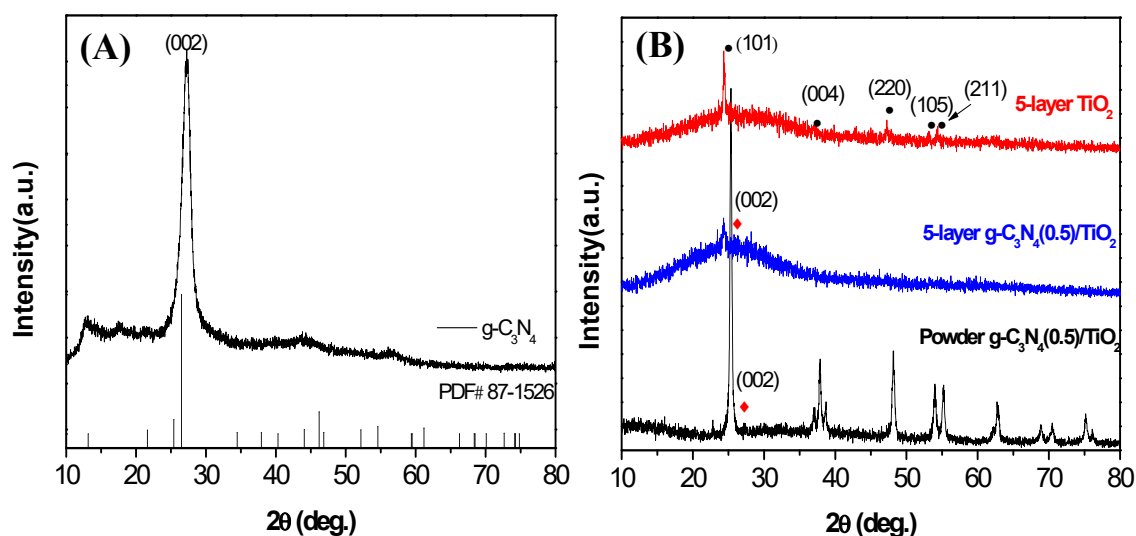


Figure 1. X-ray diffraction (XRD) patterns of (A) $\text{g-C}_3\text{N}_4$ and (B) 5-layer TiO_2 , 5-layer $\text{g-C}_3\text{N}_4(0.5)/\text{TiO}_2$, powder $\text{g-C}_3\text{N}_4(0.5)/\text{TiO}_2$.

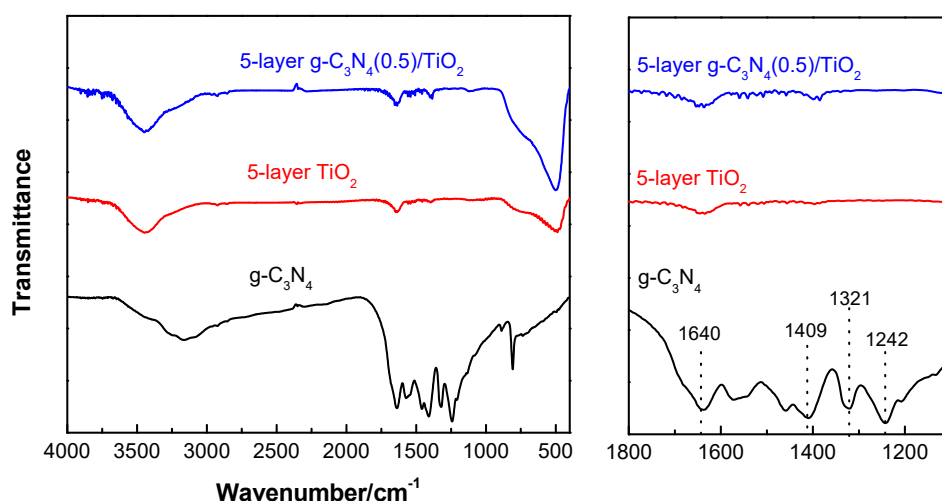


Figure 2. Fourier transform infrared (FT-IR) spectrum of $g\text{-C}_3\text{N}_4$, 5-layer TiO_2 , 5-layer $g\text{-C}_3\text{N}_4(0.5)/\text{TiO}_2$.

The surface morphology of the prepared $g\text{-C}_3\text{N}_4/\text{TiO}_2$ thin-film photocatalyst was studied by SEM, as shown in Figure 3. A flat film can be clearly seen on the glass substrate, as shown in Figure 3A–C. All the films are composed of tightly contacted irregular large and small particles, and pores are also observed at the particle interstice. Along with the increase in film thickness, the surface roughness decreases first and increases afterward. Five-layer $g\text{-C}_3\text{N}_4(0.5)/\text{TiO}_2$ has the most pores and the smallest particle size with a uniform size distribution, which indicates the presence of the photocatalytic property.

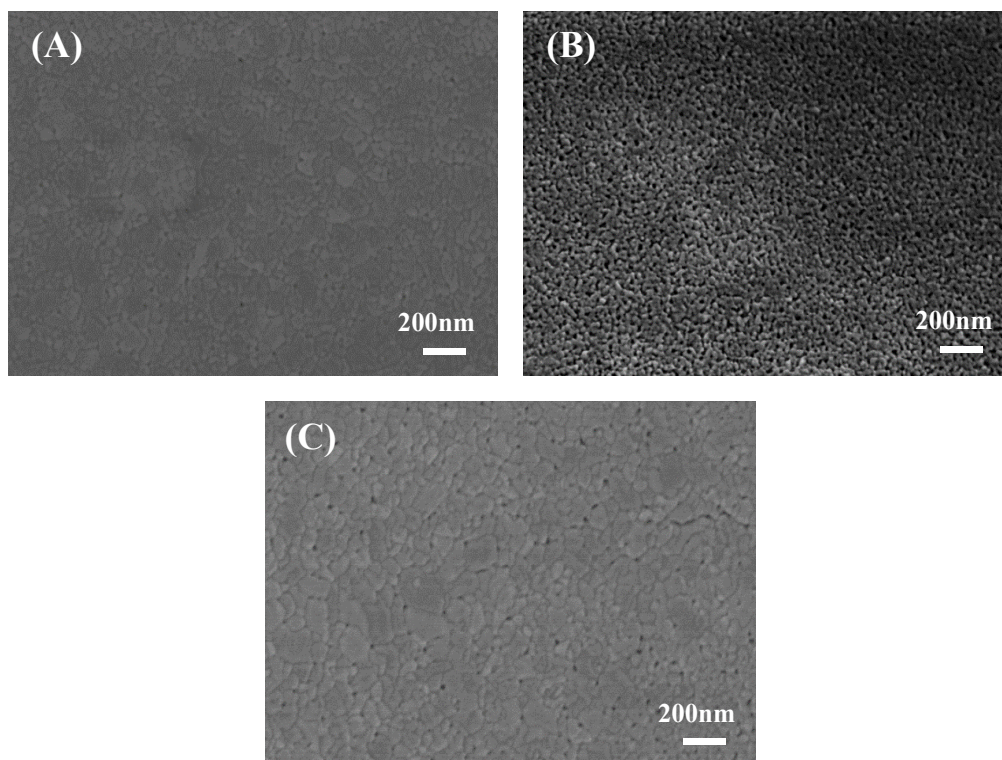


Figure 3. Scanning electron microscopy (SEM) images of different $g\text{-C}_3\text{N}_4/\text{TiO}_2$ thin-film samples: (A) 3-layer $g\text{-C}_3\text{N}_4(0.5)/\text{TiO}_2$; (B) 5-layer $g\text{-C}_3\text{N}_4(0.5)/\text{TiO}_2$; (C) 7-layer $g\text{-C}_3\text{N}_4(0.5)/\text{TiO}_2$.

3.2. Optical Property

Figure 4 shows the UV-vis diffuse spectrum of the prepared samples. As seen in Figure 4A, all the prepared photocatalysts have strong absorption in the ultraviolet region. The absorption band edge moves towards the lower direction with the increase in coating layers, which should come from the increased g-C₃N₄. The bandgap is calculated through the Tauc formula and the results are given in Figure 4B [28]. The band gaps of the g-C₃N₄-containing photocatalysts are obviously narrower than that of pristine TiO₂ and become narrower with the increase in coating layers, and the specific band gap data are shown in Table 1. These results indicate that the addition of g-C₃N₄ may improve light utilization.

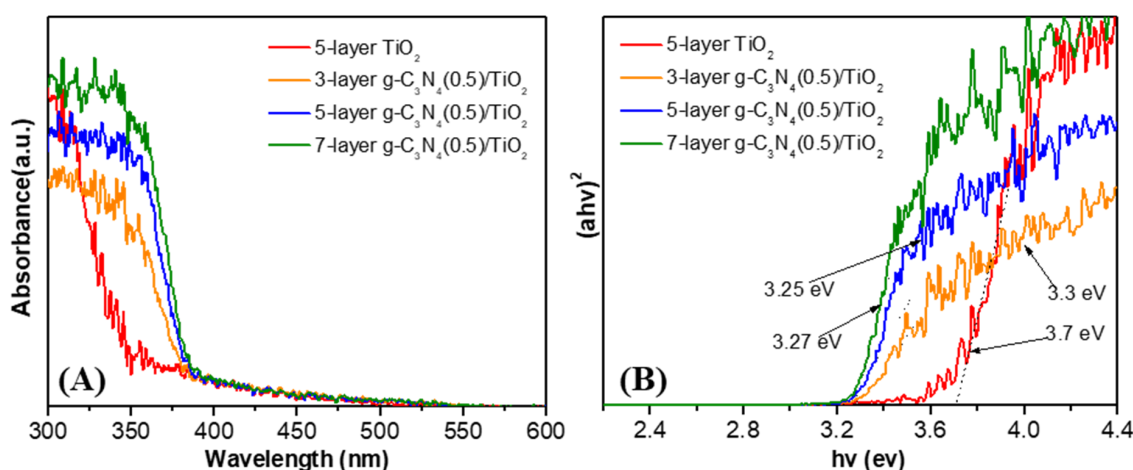


Figure 4. (A) Ultraviolet-visible diffuse reflectance spectrum (UV-vis DRS) of 5-layer TiO₂ thin film and different layers of g-C₃N₄(0.5)/TiO₂; (B) The bandgap curve after conversion of the Tauc formula.

Table 1. The energy gaps of prepared samples.

Sample Name	Energy Gap
5-layer TiO ₂	3.7 eV
3-layer g-C ₃ N ₄ (0.5)/TiO ₂	3.3 eV
5-layer g-C ₃ N ₄ (0.5)/TiO ₂	3.25 eV
7-layer g-C ₃ N ₄ (0.5)/TiO ₂	3.27 eV

3.3. Photocatalytic Activity

3.3.1. Effects of Film Thickness on the Photocatalytic Performance

The photocatalytic properties of the prepared photocatalysts were estimated by the visible-light degradation of Rh B. As shown in Figure 5A, the direct degradation of Rh B without a photocatalyst under visible light irradiation is extremely weak, which implies that the self-degradation of Rh B can be ignored. After the addition of photocatalyst, the removal rates were 5.1%, 17.9%, 31.2%, and 22.6% of Rh B under 180 min irradiation on 5-layer TiO₂, 3-layer g-C₃N₄(0.5)/TiO₂, 5-layer g-C₃N₄(0.5)/TiO₂, 7-layer g-C₃N₄(0.5)/TiO₂, respectively. These g-C₃N₄ containing-photocatalysts have much higher photocatalytic degradation efficiencies than that of pure TiO₂ thin film, which may have resulted from the synergistic effect between g-C₃N₄ and TiO₂. However, along with the increase in film layers, 7-layer g-C₃N₄(0.5)/TiO₂ has a decreased photodegradation efficiency. The kinetic rates for the photodegradation of Rh B are fitted according to the first-order reaction equation: $\ln(C_0/C)$, where k , C_0 , and C is the rate constant, initial and real-time concentration of Rh B [24]. As shown in Figure 5B, the fitting curve of the photocatalytic degradation reaction is straight and is shown below. The k values of 5-layer TiO₂, 3-layer g-C₃N₄(0.5)/TiO₂, 5-layer g-C₃N₄(0.5)/TiO₂, and 7-layer g-C₃N₄(0.5)/TiO₂

are 2.90×10^{-4} , 11.2×10^{-4} , 21.8×10^{-4} , and $13.3 \times 10^{-4} \text{ min}^{-1}$, respectively. Among them, 5-layer $\text{g-C}_3\text{N}_4(0.5)/\text{TiO}_2$ shows the best photocatalytic performance and its rate constant is nearly four times higher than that of 5-layer TiO_2 . However, the photocatalytic activity decreases with the further increase in the coating layer, and 7-layer $\text{g-C}_3\text{N}_4(0.5)/\text{TiO}_2$ demonstrates a decreased efficiency. The difference in the photocatalytic activity should come from the different characteristics of the prepared $\text{g-C}_3\text{N}_4/\text{TiO}_2$ thin-film photocatalysts such as BET specific surface and particle size. According to the results of SEM analyses, the increase in the coating layers has an influence on the particle size and porous feature, and 5-layer $\text{g-C}_3\text{N}_4(0.5)/\text{TiO}_2$ has the smallest particle size and most of the pores. This may help the access between the pollutant and the active sites, which finally improves the photocatalytic performance.

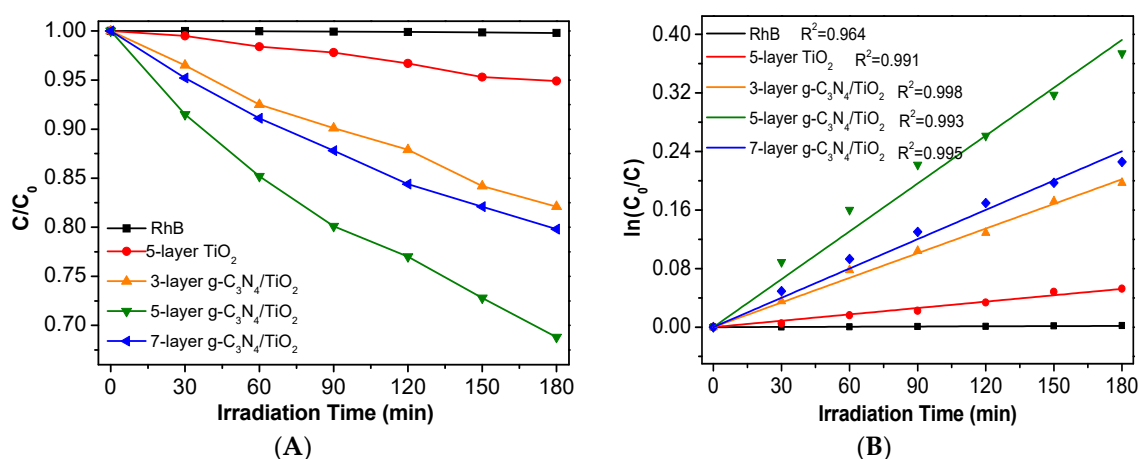


Figure 5. (A) Photocatalytic degradation of Rh B by 5-layer TiO_2 and $\text{g-C}_3\text{N}_4/\text{TiO}_2$ thin films with different spin-coating layers. (B) The first-order kinetic fitting curve of the photocatalytic degradation.

3.3.2. Effects of Film Composition on the Photocatalytic Performance

According to the above analysis, the 5-layer thin-film photocatalyst has the highest photocatalytic activity. To further investigate the composition impact on the photocatalytic performance, 5-layer photocatalysts with different quantities of $\text{g-C}_3\text{N}_4$ were prepared and the corresponding photocatalytic degradations of Rh B were done. As seen in Figure 6A, 14.3%, 18.8%, 26.3%, 31.2%, and 28.0% of Rh B were degraded after 180 min irradiation on 5-layer $\text{g-C}_3\text{N}_4(0.05)/\text{TiO}_2$, 5-layer $\text{g-C}_3\text{N}_4(0.1)/\text{TiO}_2$, 5-layer $\text{g-C}_3\text{N}_4(0.3)/\text{TiO}_2$, 5-layer $\text{g-C}_3\text{N}_4(0.5)/\text{TiO}_2$, and 5-layer $\text{g-C}_3\text{N}_4(0.7)/\text{TiO}_2$, respectively. The photodegradation rate is also simulated by the above first-order kinetic fitting, as shown in Figure 6B. The photodegradation rate k for 5-layer $\text{g-C}_3\text{N}_4(0.05)/\text{TiO}_2$, 5-layer $\text{g-C}_3\text{N}_4(0.1)/\text{TiO}_2$, 5-layer $\text{g-C}_3\text{N}_4(0.3)/\text{TiO}_2$, 5-layer $\text{g-C}_3\text{N}_4(0.5)/\text{TiO}_2$, and 5-layer $\text{g-C}_3\text{N}_4(0.7)/\text{TiO}_2$ is 9.40×10^{-4} , 11.8×10^{-4} , 16.3×10^{-4} , 21.8×10^{-4} , and $18.3 \times 10^{-4} \cdot \text{min}^{-1}$, respectively. As the histogram in Figure 6C shows, the reaction constant K increases first and decreases afterwards with the increase in composition ratio, and the standard errors are 2.1×10^{-5} , 2.4×10^{-5} , 2.5×10^{-5} , 7.1×10^{-5} , and 3.1×10^{-5} , respectively. It can be intuitively seen that 5-layer $\text{g-C}_3\text{N}_4(0.5)/\text{TiO}_2$ has the highest efficiency for Rh B degradation, which is 2.1 times more than that of 5-layer $\text{g-C}_3\text{N}_4(0.05)/\text{TiO}_2$. This indicates that the increase in $\text{g-C}_3\text{N}_4$ can definitely improve the photocatalytic activity. However, the photocatalytic activity decreases with the further increase in $\text{g-C}_3\text{N}_4$, which might come from the reduced separation efficiency of photogenerated carriers from the self-recombination on $\text{g-C}_3\text{N}_4$. The photodegradation rates on all the prepared samples are summarized in Figure 6D. As shown, both the thickness and composition of the prepared thin film have an impact on the photocatalytic activity for Rh B degradation. The best photocatalyst could be obtained using a 5-layer coating with $m(\text{g-C}_3\text{N}_4): m(\text{TiO}_2) = 0.5:1$.

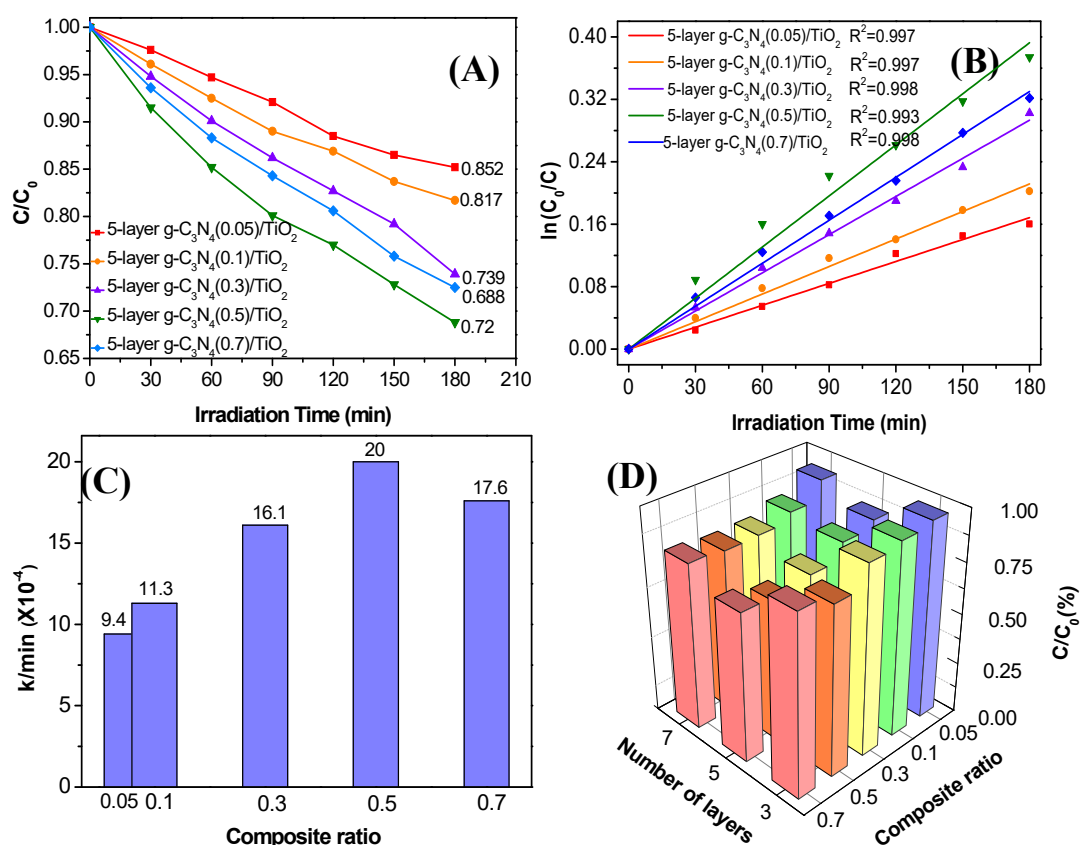


Figure 6. (A) Photocatalytic degradation of Rh B by $g\text{-C}_3\text{N}_4/\text{TiO}_2$ thin films with a different ratio. (B) The first-order kinetic fitting curve of photocatalytic degradation. (C) The histogram of reaction constants k for Rh B degradation by $g\text{-C}_3\text{N}_4/\text{TiO}_2$ thin films with different composition ratios under visible light. (D) The histogram of the three-dimensional degradation rate for all the prepared photocatalysts with different thicknesses and composition ratios.

3.4. Photocatalytic Stability

Except for the easy operation, cyclic stability is another important factor for the industrial application of thin-film photocatalysts. The antibiotic residue is another refractory pollutant in water, and the photodegradation of tetracycline hydrochloride (TC-HCl) was evaluated as the model reaction to study the photocatalytic activity as well as the stability. Five-layer $g\text{-C}_3\text{N}_4(0.5)/\text{TiO}_2$ is selected for this evaluation and the result is shown in Figure 7. A total of 25.8% TC-HCl is degraded after 180 min of visible-light irradiation, and no reduced photocatalytic performance is observed at the 2nd cycle. However, a slight decrease in the photocatalytic activity is present after the 2nd cycle, which may come from the loss of weakly attached photocatalysts. Then, no further activity loss in the other cycles is observed, indicating that the prepared thin-film photocatalyst has stability.

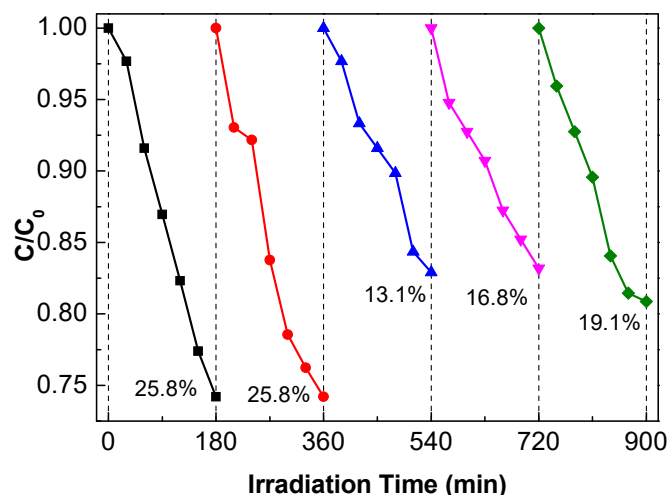


Figure 7. Cyclic stability test of the 5-layer $g\text{-C}_3\text{N}_4(0.5)/\text{TiO}_2$ photocatalytic degradation of tetracycline hydrochloride (TC-HCl).

3.5. Proposed Mechanism

The capture experiments were carried out to identify the main active substances in the photocatalytic process for understanding the corresponding reaction mechanism. Benzoquinone (BQ), tert butyl alcohol (TBA), and ethylene diamine tetraacetic acid (EDTA) were added into the Rh B solution as the trapping agent for superoxide radical ($\text{O}_2^{\bullet-}$), hydroxyl radical ($\bullet\text{OH}$), and hole (h^+), respectively [29]. As shown in Figure 8, the photocatalytic effect is significantly improved after the introduction of EDTA, which suggests that h^+ is not responsible for the photodegradation. However, the photocatalytic activity is prominently inhibited after the adding of BQ and TBA. This indicates the existence of $\bullet\text{OH}$ and $\text{O}_2^{\bullet-}$ and they both play a vital role in the above photocatalytic degradation.

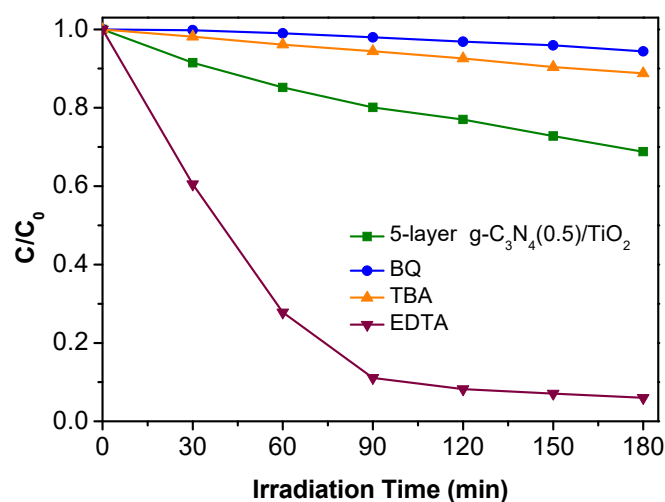


Figure 8. Photodegradation of Rh B over 5-layer $g\text{-C}_3\text{N}_4(0.5)/\text{TiO}_2$ alone and with the addition of benzoquinone (BQ), tert butyl alcohol (TBA), ethylene diamine tetraacetic acid (EDTA).

The reaction mechanism is discussed according to the above trapping experiment. If a traditional heterojunction is formed at the interface of 5-layer $g\text{-C}_3\text{N}_4(0.5)/\text{TiO}_2$, photo-generated electrons may be concentrated in the conduction band of TiO_2 , and photo-generated holes are transferred into the valence band of $g\text{-C}_3\text{N}_4$. However, the valence band energy of $g\text{-C}_3\text{N}_4$ is less than the energy required for the formation of $\bullet\text{OH}$, which cannot oxidize $\text{H}_2\text{O}/\text{OH}^-$ into $\bullet\text{OH}$ to participate

in the photocatalytic reaction. Therefore, the traditional heterojunction is not responsible for the photodegradation of Rh B, and the transport of photo-generated electrons and holes in photocatalytic reactions must follow the all-solid-state Z-scheme process, which is in correspondence with previous articles [12,18]. The transport process of all-solid-state Z-scheme heterojunction carriers is shown in Figure 9. The excited electrons in TiO_2 transfers from its conduction band to the valence band of $\text{g-C}_3\text{N}_4$. Then, the electrons are excited to the conduction band of $\text{g-C}_3\text{N}_4$ and react with the substrate to form active species. It might be pointed out that $\cdot\text{OH}$ is generally produced from the direct oxidation on the holes. However, it is difficult to completely exclude the formation of $\cdot\text{OH}$ from the consecutive reactions [30,31]. Therefore, another possible formation of $\cdot\text{OH}$ from the consecutive conversion of $\text{O}_2\cdot^-$ is also given in Figure 9.

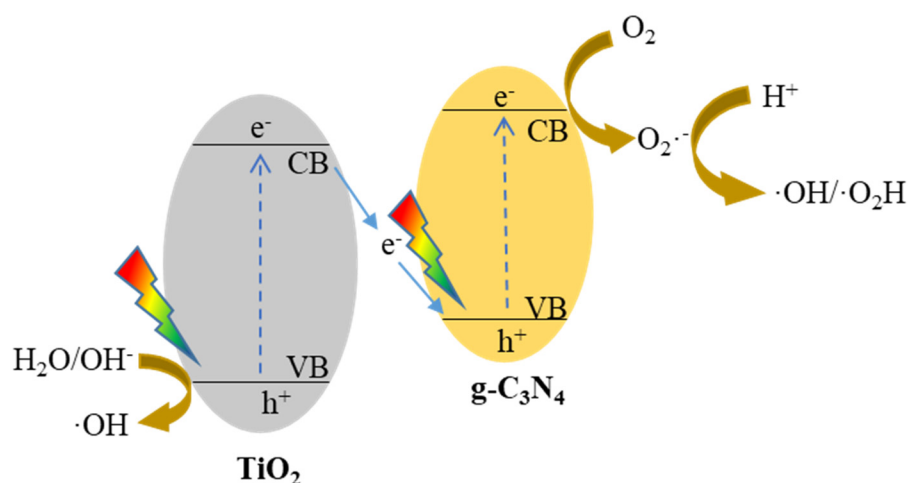


Figure 9. Proposed mechanism for the photodegradation of Rh B over 5-layer $\text{g-C}_3\text{N}_4(0.5)/\text{TiO}_2$ thin film.

4. Conclusions

In summary, all-solid-state Z-scheme $\text{g-C}_3\text{N}_4/\text{TiO}_2$ thin-film photocatalyst was successfully prepared by the facile sol-gel and spin-coating methods which showed good photocatalytic performance for the removal of colored Rh B and colorless TC-HCl with easy operation and good stability. It was found that the mass ratio of $\text{g-C}_3\text{N}_4$ to TiO_2 and coating layers had a strong influence on the photocatalytic activity. Five-layer $\text{g-C}_3\text{N}_4(0.5)/\text{TiO}_2$ showed the highest efficiency for the photodegradation and a Z-scheme mechanism was proposed. The construction of a thin-film photocatalyst may not only benefit the recovery from the reaction but also show good cyclic stability, which may be of great significance for practical application in the future.

Author Contributions: Conceptualization, Z.C. and X.L.; methodology, Z.C.; software, Q.Y.; validation, X.Y., C.L. and X.Q.; formal analysis, W.Z.; investigation, W.Z.; resources, Y.W.; data curation, T.S.; writing—original draft preparation, W.Z.; writing—review and editing, Z.X.; visualization, W.C.; supervision, X.L.; project administration, Z.C.; funding acquisition, Z.C. All authors have read and agreed to the published version of the manuscript.

Funding: This research was funded by the Zhejiang Provincial Natural Science Foundation of China, grant number LY17E020008.

Conflicts of Interest: The authors declare no conflict of interest.

References

- René, P.S.; Thomas, E.; Hofstetter, T.B.; Urs Von, G.; Bernhard, W. Global water pollution and human health. *Annu. Rev. Energy* **2010**, *35*, 109–136.
- Li, C.; Xu, Y.; Tu, W.; Chen, G.; Xu, R. Metal-free photocatalysts for various applications in energy conversion and environmental purification. *Green Chem.* **2017**, *19*, 882–899. [[CrossRef](#)]

3. Frank, S.N.; Bard, A.J. Semiconductor electrodes. 12. Photoassisted oxidations and photoelectrosynthesis at polycrystalline titanium dioxide electrodes. *J. Am. Chem. Soc.* **1977**, *99*, 4667–4675. [[CrossRef](#)]
4. Matthews, R.W. Photooxidation of organic impurities in water using thin films of titanium dioxide. *J. Phys. Chem.* **1987**, *91*, 3328–3333. [[CrossRef](#)]
5. Zhu, Y.; Chen, Z.; Gao, T.; Huang, Q.; Niu, F.; Qin, L.; Tang, P.; Huang, Y.; Sha, Z.; Wang, Y. Construction of hybrid Z-scheme Pt/CdS–TNTAs with enhanced visible-light photocatalytic performance. *Appl. Catal. B* **2015**, *163*, 16–22. [[CrossRef](#)]
6. Dong, H.; Zeng, G.; Tang, L.; Fan, C.; Zhang, C.; He, X.; He, Y. An overview on limitations of TiO₂-based particles for photocatalytic degradation of organic pollutants and the corresponding countermeasures. *Water Res.* **2015**, *79*, 128–146. [[CrossRef](#)] [[PubMed](#)]
7. Wang, X.; Zhao, Y.; Møhlhave, K.; Sun, H. Engineering the surface/interface structures of titanium dioxide micro and nano architectures towards environmental and electrochemical applications. *Nanomaterials* **2017**, *7*, 382. [[CrossRef](#)]
8. Nasr, M.; Eid, C.; Habchi, R.; Miele, P.; Bechelany, M. Recent progress on titanium dioxide nanomaterials for photocatalytic applications. *ChemSusChem* **2018**, *11*, 3023–3047. [[CrossRef](#)]
9. Tong, H.; Ouyang, S.; Bi, Y.; Umezawa, N.; Oshikiri, M.; Ye, J. Nano-photocatalytic materials: Possibilities and challenges. *Adv. Mater.* **2012**, *24*, 229–251. [[CrossRef](#)]
10. Zhang, Z.; Huang, J.; Zhang, M.; Yuan, Q.; Dong, B. Ultrathin hexagonal SnS₂ nanosheets coupled with g-C₃N₄ nanosheets as 2D/2D heterojunction photocatalysts toward high photocatalytic activity. *Appl. Catal. B* **2015**, *163*, 298–305. [[CrossRef](#)]
11. Yan, S.C.; Lv, S.B.; Li, Z.S.; Zou, Z.G. Organic–inorganic composite photocatalyst of g-C₃N₄ and TaON with improved visible light photocatalytic activities. *Dalton Trans.* **2010**, *39*, 1488–1491. [[CrossRef](#)] [[PubMed](#)]
12. Zhou, D.; Chen, Z.; Yang, Q.; Dong, X.; Zhang, J.; Qin, L. In-situ construction of all-solid-state Z-scheme g-C₃N₄/TiO₂ nanotube arrays photocatalyst with enhanced visible-light-induced properties. *Sol. Energy Mater. Sol. Cells* **2016**, *157*, 399–405. [[CrossRef](#)]
13. Wang, X.; Maeda, K.; Thomas, A.; Takane, K.; Xin, G.; Carlsson, J.M.; Domen, K.; Antonietti, M. A metal-free polymeric photocatalyst for hydrogen production from water under visible light. *Nat. Mater.* **2009**, *8*, 76–80. [[CrossRef](#)] [[PubMed](#)]
14. Low, J.; Yu, J.; Jaroniec, M.; Wageh, S.; Al-Ghamdi, A.A. Heterojunction photocatalysts. *Adv. Mater.* **2017**, *29*, 1601694. [[CrossRef](#)] [[PubMed](#)]
15. Zhou, P.; Yu, J.; Jaroniec, M. All-solid-state Z-scheme photocatalytic systems. *Adv. Mater.* **2014**, *26*, 4920–4935. [[CrossRef](#)]
16. Xu, Y.; Wen, W.; Wu, J.-M. Titania nanowires functionalized polyester fabrics with enhanced photocatalytic and antibacterial performances. *J. Hazard. Mater.* **2018**, *343*, 285–297. [[CrossRef](#)]
17. Dong, F.; Wu, L.; Sun, Y.; Fu, M.; Wu, Z.; Lee, S.C. Efficient synthesis of polymeric g-C₃N₄ layered materials as novel efficient visible light driven photocatalysts. *J. Mater. Chem.* **2011**, *21*, 15171–15174. [[CrossRef](#)]
18. Zhou, D.; Chen, Z.; Yang, Q.; Shen, C.; Tang, G.; Zhao, S.; Zhang, J.; Chen, D.; Wei, Q.; Dong, X. Facile construction of g-C₃N₄ nanosheets/TiO₂ nanotube arrays as Z-scheme photocatalyst with enhanced visible-light performance. *ChemCatChem* **2016**, *8*, 3064–3073. [[CrossRef](#)]
19. Li, J.; Chen, Z.; Fang, J.; Yang, Q.; Yang, X.; Zhao, W.; Zhou, D.; Qian, X.; Liu, C.; Shao, J. Facile synthesis of TiO₂ film on glass for the photocatalytic removal of rhodamine B and tetracycline hydrochloride. *Mater. Express* **2019**, *9*, 437–443. [[CrossRef](#)]
20. Yang, X.; Chen, Z.; Fang, J.; Yang, Q.; Zhao, W.; Qian, X.; Zhou, D.; Liu, C.; Chen, M. Freestanding 3D MoS₂ nanosheets/graphene aerogel heterostructure as a recyclable photocatalyst for efficiently degrading antibiotic residues. *Mater. Lett.* **2019**, *252*, 5–7. [[CrossRef](#)]
21. Wang, D.; Xiao, L.; Luo, Q.; Li, X.; An, J.; Duan, Y. Highly efficient visible light TiO₂ photocatalyst prepared by sol–gel method at temperatures lower than 300 °C. *J. Hazard. Mater.* **2011**, *192*, 150–159. [[CrossRef](#)] [[PubMed](#)]
22. Tao, W.; Wang, M.; Ali, R.; Nie, S.; Zeng, Q.; Yang, R.; Lau, W.-M.; He, L.; Tang, H.; Jian, X. Multi-layered porous hierarchical TiO₂/g-C₃N₄ hybrid coating for enhanced visible light photocatalysis. *Appl. Surf. Sci.* **2019**, *495*, 143435. [[CrossRef](#)]
23. Li, J.; Zhang, M.; Li, Q.; Yang, J. Enhanced visible light activity on direct contact Z-scheme g-C₃N₄-TiO₂ photocatalyst. *Appl. Surf. Sci.* **2017**, *391*, 184–193. [[CrossRef](#)]

24. Yan, H.; Yang, H. TiO₂-g-C₃N₄ composite materials for photocatalytic H₂ evolution under visible light irradiation. *J. Alloy. Compd.* **2011**, *509*, L26–L29. [[CrossRef](#)]
25. Ye, L.; Liu, J.; Jiang, Z.; Peng, T.; Zan, L. Facets coupling of BiOBr-g-C₃N₄ composite photocatalyst for enhanced visible-light-driven photocatalytic activity. *Appl. Catal. B* **2013**, *142*, 1–7. [[CrossRef](#)]
26. Alvarez, K.M.; Alvarado, J.; Soto, B.S.; Hernandez, M.A. Synthesis of TiO₂ nanoparticles and TiO₂-Zeolite composites and study of optical properties and structural characterization. *Optik* **2018**, *169*, 137–146. [[CrossRef](#)]
27. Zhang, L.; Xing, Z.; Zhang, H.; Li, Z.; Wu, X.; Zhang, X.; Zhang, Y.; Zhou, W. High thermostable ordered mesoporous SiO₂-TiO₂ coated circulating-bed biofilm reactor for unpredictable photocatalytic and biocatalytic performance. *Appl. Catal. B* **2016**, *180*, 521–529. [[CrossRef](#)]
28. Guli, M.; Yao, J.; Zhao, J.; Rao, W.; Xiao, L.; Tian, H. Preparation and characterization of TiO₂ anode film with spinodal phase separation structure in dye-sensitized solar cells. *Opt. Mater.* **2013**, *35*, 2175–2182. [[CrossRef](#)]
29. Qian, X.; Chen, Z.; Yang, X.; Zhao, W.; Liu, C.; Sun, T.; Zhou, D.; Yang, Q.; Wei, G.; Fan, M. Perovskite cesium lead bromide quantum dots: A new efficient photocatalyst for degrading antibiotic residues in organic system. *J. Clean. Prod.* **2019**, *249*, 119335. [[CrossRef](#)]
30. Gaya, U.I.; Abdullah, A.H. Heterogeneous photocatalytic degradation of organic contaminants over titanium dioxide: a review of fundamentals, progress and problems. *J. Photochem. Photobiol. C* **2008**, *9*, 1–12. [[CrossRef](#)]
31. Chen, S.; Zhang, S.; Zhao, W.; Liu, W. Study on the photocatalytic activity of TiN/TiO₂ nanoparticle formed by ball milling. *J. Nanopart. Res.* **2009**, *11*, 931–938. [[CrossRef](#)]



© 2020 by the authors. Licensee MDPI, Basel, Switzerland. This article is an open access article distributed under the terms and conditions of the Creative Commons Attribution (CC BY) license (<http://creativecommons.org/licenses/by/4.0/>).